Controlled Islanding Strategy Considering Uncertainty of Renewable Energy Sources Based on Chance-constrained Model

Shengyuan Liu, *Student Member*, *IEEE*, Tianhan Zhang, *Student Member*, *IEEE*, Zhenzhi Lin, *Member*, *IEEE*, Yilu Liu, *Fellow*, *IEEE*, Yi Ding, *Member*, *IEEE*, and Li Yang, *Member*, *IEEE*

***Abstract*—Controlled islanding plays an essential role in preventing the blackout of power systems. Although there are several studies on this topic in the past, no enough attention is paid to the uncertainty brought by renewable energy sources (RESs) that may cause unpredictable unbalanced power and the observability of power systems after islanding that is essential for back-up black-start measures. Therefore, a novel controlled islanding model based on mixed-integer second-order cone and chance-constrained programming (MISOCCP) is proposed to address these issues. First, the uncertainty of RESs is characterized by their possibility distribution models with chance constraints, and the requirements, e. g., system observability, for rapid back-up black-start measures are also considered. Then, a law of large numbers (LLN) based method is employed for converting the chance constraints into deterministic ones and reformulating the non-convex model into convex one. Finally, case studies on the revised IEEE 39-bus and 118-bus power systems as well as the comparisons among different models are given to demonstrate the effectiveness of the proposed model. The results show that the proposed model can result in less unbalanced power and better observability after islanding compared with other models.**

***Index Terms*—Controlled islanding, second-order cone, chance-constrained programming, renewable energy source (RES), black-start, observability.**

I. Introduction

With the continuous expansion of power systems and the ever-increasing penetration of renewable energy sources (RESs) in recent years, the monitoring and control of power systems have become more and more complex [1], [2]. Therefore, a rapid spread of faults may be caused in the case of serious disturbances and thereby endanger the overall stability of power systems. Although a single event may not be enough to destabilize the power system, the cumulative effects can be catastrophic. It is shown in research and analysis of major power failure events that the timely and accurate control measures according to the operation state of power systems can effectively improve the stability and mitigate the risks of the power system failure [3]. Therefore, it is significant to take timely measures to curb the further expansion of faults in order to prevent the occurrence of disasters in bulk power systems. The controlled islanding strategy is to obtain the real-time state of power systems through the wide-area measurement system (WAMS) during oscillation and then get the optimal splitting boundary online. The current methods for achieving the optimal controlled islanding strategy can be divided into three categories, i. e., methods based on slow coherency theory, artificial intelligence, and graph theory.

The basic idea of the methods based on slow coherency theory [4]-[6] is to extract the dynamic model of power systems and analyze the "weak connection" between generator clusters, then to search the islanding cross-sections in the region with a weak connection. In [6], METIS, a software package for graph segmentation, is used to divide the simplified system into several isolated subsystems, and the parallel operation and recovery operation are carried out to obtain the islanding scheme corresponding to the original power system. These methods can effectively reduce the scale of the feasible region and make the physical meaning much clearer. However, searching for the optimal islanding cross-sections of power systems is a non-deterministic polynomial (NP) complete problem. The methods based on artificial intelligence such as grey wolf optimized artificial neural network (GWO-ANN) and ant colony method [7], [8] are suitable for solving NP-complete problems, and these methods possess strong adaptability but are limited by the size of power systems, high complexity, and heavy computation burden. The methods based on graph theory mainly include network simplification [9] and fast network partitioning methods based on mixed-integer linear programming (MILP) [10]-

Manuscript received: June 28, 2020; revised: October 25, 2020; accepted: December 29, 2020. Date of CrossCheck: December 29, 2020. Date of online publication: April 5, 2021.

This work was supported by the National Natural Science Foundation of China (No. 51777185), National Key R&D Program of China (No. 2016YFB0900100), and Zhejiang University Academic Award for Outstanding Doctoral Candidates.

S. Liu, T. Zhang, Z. Lin (corresponding author), Y. Ding, and L. Yang are with the School of Electrical Engineering, Zhejiang University, Hangzhou 310027, China, S. Liu is also with the Department of Electrical Engineering and Computer Science, University of Tennessee, Knoxville, TN 37996, USA, and Z. Lin is also with the School of Electrical Engineering, Shandong University, Jinan 250061, China (e-mail: eelsy@zju.edu.cn; eezhangth@zju.edu.cn; linzhenzhi@zju.edu.cn; yiding@zju.edu.cn; eeyangli@zju.edu.cn).

Y. Liu is with the Department of Electrical Engineering and Computer Science, University of Tennessee, Knoxville, TN 37996, USA, and she is also with Electrical and Electronics Systems Research Division, Oak Ridge National Laboratory, Oak Ridge, TN 37830, USA (e-mail: liu@utk.edu).

DOI: 10.35833/MPCE.2020.000411

[12] or spectral clustering [13]-[15]. The basic idea of the network simplification method [9] is to use graph theory to simplify and adjust the given power system to reduce the computation time. Different from the network simplification method, the fast network partitioning method does not simplify a given power system but rather divides it directly by the dynamic characteristics. In [9], a three-phase splitting strategy for large-scale power systems is proposed based on the ordered binary decision diagram (OBDD). Spectral and multi-level kernel *k*-means methods are proposed in [13]-[15], and the controlled islanding problem is converted as a weighted undirected graph segmentation problem to achieve the minimum power flow distribution. In [10]-[12], the graph segmentation is first modeled as MILP problems, which can be solved efficiently by using the direct power flow method.

The development of RESs is an irresistible trend and the uncertainty of RESs would cause unpredictable fluctuations in power generation. Therefore, there are potential hazards for successful islanding, since traditional islanding strategies are all based on the condition that the power generation can be dispatched. To address this issue, several optimization models such as robust optimization and stochastic optimization models considering the uncertainty of RESs are proposed [16]-[19]. In [16], the robust optimization model is presented to obtain the optimal operation schedule for power grid connection. In [17], a robust secondary cooperative control model is introduced for islanded microgrids. In [18], a robust scheduling model for the microgrid considering islanding constraints is presented to minimize the total operation cost. In [19], a controlled islanding strategy based on robust optimization programming that considers the online coherency identification and the fluctuations of RESs is proposed for minimizing the load shedding after islanding. Indeed, the robust optimization model is a good way to deal with the uncertainty of RESs, while its results are too conservative since it always considers the worst situation. In other words, the existence of an extreme situation will greatly influence the final islanding strategy, which causes an unnecessary loss in most of normal situations.

Given this background, this study proposes a controlled islanding model based on mixed-integer second-order cone and chance-constrained programming (MISOCCP), which considers the uncertainty of RESs with possibility distribution models. The proposed model can be converted into a form of convex optimization that can be solved efficiently. The contributions of this study are summarized as follows.

1) A controlled islanding model is built considering the nonlinearity of power systems, e.g., reactive power balance, connectivity, and coherency, and the second-order cone (SOC) relation is presented to transform the model into a convex optimization problem, which can be solved by commercial solver efficiently. Compared with the oversimplified linear controlled islanding model that does not consider the nonlinearity of power systems, the proposed model can obtain more suitable islanding boundaries with less unbalanced power.

2) The deterministic conversion method based on law of large numbers (LLN) is utilized to reformulate the chance constraints associated with the uncertainty of RESs to the deterministic ones. Compared with the existing models, the proposed model can take RESs into consideration. Meanwhile, compared with the controlled islanding model based on the robust optimization which is quite conservative, the proposed model can describe the uncertainty of RESs by possibility distribution with a given confidence level, resulting in less unbalance power.

3) The proposed model is tested in IEEE 39-bus and IEEE 118-bus power systems, and the comparison among different models are also given. The observability of power systems after islanding is considered in the proposed model. Compared with other models, the proposed model can guarantee the observability of each bus after islanding, which is essential for back-up black-start measures in case of the unexpected islanding failure due to the uncertainty of RESs or other issues.

II. Controlled Islanding Model Based on MISOCCP Considering Uncertainty of RESs

A. Objective Function for Controlled Islanding Model with Uncertainty of RESs

Generally, the unbalanced power after controlled islanding is regarded as a crucial index for the operation reliability of power utilities. The less the unbalanced power after controlled islanding is, the better the islanding strategy will be. Therefore, different RES generation and load variation scenarios are generated by sampling from their possibility distribution functions in this study for evaluating the performance of the controlled islanding model comprehensively. It is worth mentioning that the unbalanced power after islanding in different scenarios will be different, thus this study aims to minimize the average unbalanced power in different RES generation and load variation scenarios, which can be denoted as:

$$\min \frac{1}{N_{\text{samp}}} \sum_{\lambda=1}^{N_{\text{samp}}} \sum_{i=1}^{N_{\text{bus}}} P_{\text{UB},i,\lambda} = \sum_{\lambda=1}^{N_{\text{samp}}} \sum_{i=1}^{N_{\text{bus}}} (P_{\text{gen},i,\lambda}^{\text{up}} + \tilde{P}_{\text{w},i,\lambda} + \tilde{P}_{\text{s},i,\lambda} - \tilde{P}_{\text{L},i,\lambda}) \quad (1)$$

where N_{samp} and N_{bus} are the numbers of sampling times and buses, respectively; $P_{\text{UB},i,\lambda}$ is the unbalanced active power output of bus i in the λ^{th} sampling scenario; $P_{\text{gen},i,\lambda}^{\text{up}}$ is the up-regulation active power output of generator at bus i in the λ^{th} sampling scenario; and $\tilde{P}_{\text{w},i,\lambda}$, $\tilde{P}_{\text{s},i,\lambda}$, and $\tilde{P}_{\text{L},i,\lambda}$ are the errors between actual and predicted active power outputs of wind power generator, solar power generator, and the load at bus i in the λ^{th} sampling scenario, respectively.

B. Chance Constraints Considering Uncertainties of RESs and Loads

The fluctuations and uncertainties of RESs and loads would influence the power balance. Therefore, the chance-constrained programming is utilized to model the power balance by constraints with given confidence levels to mitigate the conservativeness of robust programming [20]. Thus, the chance constraints with the uncertainties of RESs and loads considered can be represented as:

$$\Pr\left[\sum_{i=1}^{N_{\text{bus}}} P_{\text{gen},i}^{\text{up}} + \sum_{i=1}^{N_{\text{bus}}} (\tilde{P}_{\text{w},i} + \tilde{P}_{\text{s},i} - \tilde{P}_{\text{L},i}) + \sum_{i=1}^{N_{\text{bus}}} P_{\text{UB},i} \geq 0\right] \geq \tau_1 \quad (2)$$

$$\Pr\left[\sum_{i=1}^{N_{\text{bus}}} Q_{\text{gen},i}^{\text{up}} + \sum_{i=1}^{N_{\text{bus}}} (\tilde{Q}_{\text{w},i} + \tilde{Q}_{\text{s},i} - \tilde{Q}_{\text{L},i}) + \sum_{i=1}^{N_{\text{bus}}} Q_{\text{UB},i} \geq 0\right] \geq \tau_2 \quad (3)$$

$$\Pr\left[\sum_{i=1}^{N_{\text{bus}}} P_{\text{gen},i}^{\text{down}} - \sum_{i=1}^{N_{\text{bus}}} (\tilde{P}_{\text{w},i} + \tilde{P}_{\text{s},i} - \tilde{P}_{\text{L},i}) + \sum_{i=1}^{N_{\text{bus}}} P_{\text{UB},i} \geq 0\right] \geq \tau_3 \quad (4)$$

$$\Pr\left[\sum_{i=1}^{N_{\text{bus}}} Q_{\text{gen},i}^{\text{down}} - \sum_{i=1}^{N_{\text{bus}}} (\tilde{Q}_{\text{w},i} + \tilde{Q}_{\text{s},i} - \tilde{Q}_{\text{L},i}) + \sum_{i=1}^{N_{\text{bus}}} Q_{\text{UB},i} \geq 0\right] \geq \tau_4 \quad (5)$$

where $\Pr(\cdot)$ and τ_k ($k=1, 2, 3, 4$) are the possibility function and the corresponding confidence level, respectively; $P_{\text{gen},i}^{\text{up}}$ and $Q_{\text{gen},i}^{\text{up}}$ are the up-regulation active and reactive power outputs of the generator at bus i, respectively; $\tilde{P}_{\text{w},i}$, $\tilde{P}_{\text{s},i}$, and $\tilde{P}_{\text{L},i}$ are the errors between actual and predicted active power outputs of wind power generator, solar power generator, and load at bus i, respectively; $P_{\text{UB},i}$ and $Q_{\text{UB},i}$ are the unbalanced active and reactive power outputs of bus i, respectively; $\tilde{Q}_{\text{w},i}$, $\tilde{Q}_{\text{s},i}$, and $\tilde{Q}_{\text{L},i}$ are the errors between actual and predicted reactive power outputs of wind power generator, solar power generator, and the load at bus i, respectively; and $P_{\text{gen},i}^{\text{down}}$ and $Q_{\text{gen},i}^{\text{down}}$ are the down-regulation active and reactive power outputs of the generator at bus i, respectively. The values of τ_k can be used to control the confidence level and can be adjusted by system operators according to their requirements. In particular, the values can be set to be 100% if the extreme scenarios are required to be avoided completely, which means the chance-constrained programming is degraded as the robust programming.

It can be seen that constraints (2) - (5) are chance-constrained; thus it cannot be solved directly. Chance constraints could be converted into deterministic ones through analytical derivation method from the probabilistic models of random variables [21]-[23]. However, the analytical derivation method can only be employed for a single random variable, while it is helpless for multiple random variables as in this study. Hence, a deterministic conversion method based on LLN is proposed, which relies on the sampling rather than the complex derivation of probabilistic models. In probability theory, the LLN establishes the relationship between the probability of an event and its incidence after performing the same trials for a large number of times. According to this law, the incidence of an event divided by the total trial count should be close to its true probability and will converge to the probability as the number of trials approaches infinity [24]. In other words, the LNN guarantees stable long-term results for random events [25]. In brief, the proposed model considering the uncertainty of RESs is a chance-constrained model, and the proposed model is utilized to convert the chance constraints into deterministic constraints so as to solve the model effectively.

Therefore, the chance constraints (2)-(5) are converted into the deterministic ones by the proposed model as:

$$\sum_{i=1}^{N_{\text{bus}}} (P_{\text{gen},i,\lambda}^{\text{up}} + \tilde{P}_{\text{w},i,\lambda} + \tilde{P}_{\text{s},i,\lambda} - \tilde{P}_{\text{L},i,\lambda} + P_{\text{UB},i,\lambda}) \geq -M(1-\eta_{1,\lambda}) \quad (6)$$

$$\sum_{i=1}^{N_{\text{bus}}} (Q_{\text{gen},i,\lambda}^{\text{up}} + \tilde{Q}_{\text{w},i,\lambda} + \tilde{Q}_{\text{s},i,\lambda} - \tilde{Q}_{\text{L},i,\lambda} + Q_{\text{UB},i,\lambda}) \geq -M(1-\eta_{2,\lambda}) \quad (7)$$

$$\sum_{i=1}^{N_{\text{bus}}} (P_{\text{gen},i,\lambda}^{\text{down}} - \tilde{P}_{\text{w},i,\lambda} - \tilde{P}_{\text{s},i,\lambda} + \tilde{P}_{\text{L},i,\lambda} - P_{\text{UB},i,\lambda}) \geq -M(1-\eta_{3,\lambda}) \quad (8)$$

$$\sum_{i=1}^{N_{\text{bus}}} (Q_{\text{gen},i,\lambda}^{\text{down}} - \tilde{Q}_{\text{w},i,\lambda} - \tilde{Q}_{\text{s},i,\lambda} + \tilde{Q}_{\text{L},i,\lambda} - Q_{\text{UB},i,\lambda}) \geq -M(1-\eta_{4,\lambda}) \quad (9)$$

$$\sum_{\lambda=1}^{N_{\text{samp}}} \eta_{k,\lambda} \geq \tau_k N_{\text{samp}} \quad k=1,2,3,4 \quad (10)$$

where $\eta_{k,\lambda}$ is the binary variable in the λ^{th} sampling scenario; M is a number that is big enough; $Q_{\text{gen},i,\lambda}^{\text{up}}$ is the up-regulation reactive power output of the generator at bus i in the λ^{th} sampling scenario; and $\tilde{Q}_{\text{w},i,\lambda}$, $\tilde{Q}_{\text{s},i,\lambda}$, and $\tilde{Q}_{\text{L},i,\lambda}$ are the errors between actual and predicted reactive power outputs of wind power generator, solar power generator, and the load at bus i in the λ^{th} sampling scenario, respectively; $Q_{\text{UB},i,\lambda}$ is the unbalanced reactive power output of bus i in the λ^{th} sampling scenario; and $P_{\text{gen},i,\lambda}^{\text{down}}$ and $Q_{\text{gen},i,\lambda}^{\text{down}}$ are the down-regulation active and reactive power outputs of generator at bus i in the λ^{th} sampling scenario, respectively.

It is worth mentioning that the values of $\tilde{P}_{\text{w},i,\lambda}$, $\tilde{P}_{\text{s},i,\lambda}$, $\tilde{P}_{\text{L},i,\lambda}$, $\tilde{Q}_{\text{w},i,\lambda}$, $\tilde{Q}_{\text{s},i,\lambda}$, and $\tilde{Q}_{\text{L},i,\lambda}$ are determined through their probability distribution functions, i. e., Weibull distribution function for wind power generation [26], Beta distribution function for solar power generation [27], and Gaussian distribution function for load variation [28]. It can be seen that if the left sides of constraints (6)-(9) are smaller than 0, then $\eta_{k,\lambda}=0$. Given the confidence level τ_k, $\eta_{k,\lambda}$ should be equal to 1 for $\tau_k N_{\text{samp}}$ times at least for satisfying constraint (10), which means the left sides of constraints (6)-(9) should be greater than zero for $\tau_k N_{\text{samp}}$ times. According to the LLN, constraints (6)-(10) are equivalent to constraints (2)-(5) when N_{samp} is large enough.

C. Connectivity and Coherency Constraints

On one hand, a given power system would be divided into several sub-power systems after controlled islanding, and each sub-power system should maintain its connectivity so that there is no isolated bus. On the other hand, some generators are required to be disconnected from each other according to the results of coherency identification. In other words, the generators that have synchronous rotor angle trajectories are the coherent ones, which should be kept on the same island. However, some generators have asynchronous rotor angle trajectories after disturbances, which results in incoherence, and should be divided into different islands. To address these issues, an artificial power flow method (APFM) [10] is utilized to guarantee the connectivity and coherency within each island and the incoherency of generators among different islands as:

$$P_{ij}^{\text{con}} = y_{ij}(\delta_i^{\text{con}} - \delta_j^{\text{con}})/X^{\text{f}} \quad (11)$$

$$\sum_{j=1,j\neq i}^{N_{\text{bus}}} P_{ij}^{\text{con}} = -P_{\text{L}}^{\text{con}} \quad i \in \Omega_{\text{gen}} - \Omega_{\text{slackgen}}^{\text{con}} \quad (12)$$

$$\sum_{j=1,j\neq i}^{N_{\text{bus}}} P_{ij}^{\text{con}} = P_{\text{gen},i}^{\text{con}} \quad i \in \Omega_{\text{slackgen}}^{\text{con}} \tag{13}$$

$$P_{ij}^{\text{dis}} = y_{ij}(\delta_i^{\text{dis}} - \delta_j^{\text{dis}})/X^{\text{f}} \tag{14}$$

$$P_{ij}^{\text{dis}} = 0 \tag{15}$$

$$\delta_i^{\text{dis}} = \delta_{k_1}^{\text{dis}} \quad i \in \Omega_{k_1}^{\text{island}} \tag{16}$$

where P_{ij}^{con}, $P_{\text{gen},i}^{\text{con}}$, δ_i^{con}, and δ_j^{con} are the fictitious power flow of the line between buses i and j, the fictitious power output of artificial slack generators (ASGs) at bus i, and the fictitious phase angles of buses i and j that are involved to build the connectivity constraints, respectively; y_{ij} is a binary variable, which equals to 1 when the line between buses i and j is connected and 0 otherwise; Ω_{gen} is the set of all generators; P_{ij}^{dis}, δ_i^{dis}, and δ_j^{dis} are the fictitious power flow of the line between buses i and j and the fictitious phase angles of buses i and j that are involved to build the coherency constraints, respectively; $\Omega_{\text{slackgen}}^{\text{con}}$ is the set of ASGs and only one ASG is assigned for each island; $\Omega_{k_1}^{\text{island}}$ is the set of the generators on the k_1^{th} island; $P_{\text{L}}^{\text{con}}$ and X^{f} are the artificial load and reactance, respectively, and both of them can be set as small constants; and $\delta_{k_1}^{\text{dis}}$ is the non-equal constants. δ_i^{con}, δ_j^{con}, and $P_{\text{gen},i}^{\text{con}}$ are variables that can be any values for satisfying constraints (11)-(13). It can be seen from constraints (11)-(13) that there is an artificial load for every bus, except for the buses with ASGs. Besides, the artificial load at each bus can be supplied by ASGs via transmission lines. Therefore, the connectivity can be guaranteed for each island as long as there are feasible solutions for δ_i^{con}, δ_j^{con}, and $P_{\text{gen},i}^{\text{con}}$. It is noted that $\Omega_{k_1}^{\text{island}}$ is known in the coherency identification stage and the values of $\delta_{k_1}^{\text{dis}}$ are given in advance.

However, constraints (11) and (14) are nonlinear, thus the "big-M" method [29], [30] is utilized to linearize them as:

$$P_{ij}^{\text{a,dis}} = (\delta_i^{\text{dis}} - \delta_j^{\text{dis}})/X_{\text{f}} \tag{17}$$

$$-M(1-y_{ij}) \leq P_{ij}^{\text{dis}} - P_{ij}^{\text{a,dis}} \leq M(1-y_{ij}) \tag{18}$$

$$P_{ij}^{\text{a,con}} = (\delta_i^{\text{con}} - \delta_j^{\text{con}})/X_{\text{f}} \tag{19}$$

$$-M(1-y_{ij}) \leq P_{ij}^{\text{con}} - P_{ij}^{\text{a,con}} \leq M(1-y_{ij}) \tag{20}$$

where the superscript a represents the variables are auxiliary variables. It should be emphasized that constraints (11)-(16) just establish several artificial power flow equations for modeling the connectivity and coherency constraints with a mathematical form, and they have no relationship with the real physical power flow. Similarly, P_{ij}^{con}, δ_i^{con}, δ_j^{con}, $P_{\text{gen},i}^{\text{con}}$, P_{ij}^{dis}, δ_i^{dis}, and δ_j^{dis} are only fictitious or auxiliary variables for building the connectivity and coherency constraints, and they have no relationship with the actual state variables in power systems. In the actual application, the coherent generator groups are determined first, and then the constraints will guarantee the connectivity of each island and the coherency of generators with each island based on the determination results.

D. Black-start Constraints

It is known that black-start is a back-up measure for restoring power systems in case controlled islanding fails to prevent a blackout. This situation is worth considering since the power balance in power systems could be threatened with higher and higher penetration of RESs. Therefore, it is necessary to consider the requirements that contribute to the back-up black-start stage when making a controlled islanding strategy.

First, it is essential for operators to monitor the real-time states of power systems, e.g., the voltage, phase angle, frequency, and active/reactive power generation/consumption at each bus. In other words, the observability of power systems should be guaranteed so that the important electrical state variables can be obtained. This requirement can be modeled as:

$$\sum_{j=1,j\neq i}^{N_{\text{bus}}} y_{ij} o_j + o_i \geq 1 \tag{21}$$

where o_i is the binary variable that indicates the locations of phasor measurement units (PMUs), and $o_i = 1$ if there is a PMU deployed at bus i and $o_i = 0$ otherwise. Constraint (21) means there is at least one PMU deployed at bus i or the buses that adjoin bus i. Since the electrical state variables of a bus can be measured directly if a PMU is deployed or can be calculated indirectly if a PMU is deployed adjacently, constraint (21) can guarantee the observability of the given power system.

Second, it is obvious that every black-start generator belongs to the black-start zone formed by itself, and each bus belongs to and only belongs to one black-start zone. This requirement can be modeled as:

$$\Theta_{jj} = 1 \quad j \in \Omega_{\text{BS}} \tag{22}$$

$$\sum_{j\in\Omega_{\text{BS}}} \Theta_{ij} = 1 \tag{23}$$

where Θ_{ij} is the binary variable that indicates the memberships of buses in black-start zones, and $\Theta_{ij} = 1$ if bus i is in the black-start zone formed by black-start generator j and $\Theta_{ij} = 0$ otherwise; and Ω_{BS} is the set of black-start generators.

Third, each black-start zone after islanding cannot be too small in practice, since a larger black-start zone is better for the stability and power balance [6] within it, so as to help accelerate the black-start process. This requirement can be represented as:

$$\sum_{i=1}^{N_{\text{bus}}} \Theta_{ij} \geq N_{\text{BS}}^{\min} \tag{24}$$

where $N_{\text{BS}}^{\min}$ is the minimum number of buses in each black-start zone. Finally, some critical lines such as transformer branches should remain connected at the islanding stage, so as to accelerate the back-up black-start process in case it is required. This requirement can be represented as:

$$y_{ij} = y_{ji} = 1 \quad (i,j) \in \Omega_{\text{T}} \tag{25}$$

where Ω_{T} is the set of transformer branches.

E. Basic Physical Constraints

Besides the aforementioned new constraints, several basic physical constraints are also required as follows.

$$\begin{cases} P_i = \sum_{j=1,j\neq i}^{N_{\text{bus}}} P_{ij} \\ Q_i = \sum_{j=1,j\neq i}^{N_{\text{bus}}} Q_{ij} \end{cases} \tag{26}$$

$$P_i - P_{\mathrm{UB},i} = P_{\mathrm{gen},i} + P_{\mathrm{gen},i}^{\mathrm{up}} - P_{\mathrm{gen},i}^{\mathrm{down}} + \hat{P}_{\mathrm{w},i} + \hat{P}_{\mathrm{s},i} - \hat{P}_{\mathrm{L},i} \quad (27)$$

$$Q_i - Q_{\mathrm{UB},i} = Q_{\mathrm{gen},i} + Q_{\mathrm{gen},i}^{\mathrm{up}} - Q_{\mathrm{gen},i}^{\mathrm{down}} + \hat{Q}_{\mathrm{w},i} + \hat{Q}_{\mathrm{s},i} - \hat{Q}_{\mathrm{L},i} \quad (28)$$

$$0 \le P_{\mathrm{gen},i}^{\mathrm{up}} \le \min\{\kappa_i^{\mathrm{P}} P_{\mathrm{gen},i}^{\max},\ P_{\mathrm{gen},i}^{\max} - P_{\mathrm{gen},i}\} \quad (29)$$

$$0 \le Q_{\mathrm{gen},i}^{\mathrm{up}} \le \min\{\kappa_i^{\mathrm{Q}} Q_{\mathrm{gen},i}^{\max},\ Q_{\mathrm{gen},i}^{\max} - P_{\mathrm{gen},i}\} \quad (30)$$

$$0 \le P_{\mathrm{gen},i}^{\mathrm{down}} \le \min\{\kappa_i^{\mathrm{P}} P_{\mathrm{gen},i}^{\max},\ P_{\mathrm{gen},i} - P_{\mathrm{gen},i}^{\min}\} \quad (31)$$

$$0 \le Q_{\mathrm{gen},i}^{\mathrm{down}} \le \min\{\kappa_i^{\mathrm{Q}} Q_{\mathrm{gen},i}^{\max},\ Q_{\mathrm{gen},i} - Q_{\mathrm{gen},i}^{\min}\} \quad (32)$$

$$P_{ij} = y_{ij}[G_{ij}V_i^2 - V_iV_j(G_{ij}\cos\theta_{ij} + B_{ij}\sin\theta_{ij})] \quad (33)$$

$$Q_{ij} = y_{ij}[V_iV_j(G_{ij}\sin\theta_{ij} - B_{ij}\cos\theta_{ij}) - G_{ij}V_i^2] \quad (34)$$

$$\theta_{ij} = \theta_i - \theta_j \quad (35)$$

where P_i and Q_i are the injected active and reactive power of bus i, respectively; $\hat{P}_{\mathrm{w},i}$, $\hat{P}_{\mathrm{s},i}$, and $\hat{P}_{\mathrm{L},i}$ are the predicted active power outputs of wind power generator, solar power generator, and the load at bus i, respectively; $\hat{Q}_{\mathrm{w},i}$, $\hat{Q}_{\mathrm{s},i}$, and $\hat{Q}_{\mathrm{L},i}$ are the predicted reactive power outputs of wind power generator, solar power generator, and the load at bus i, respectively; $P_{\mathrm{gen},i}$ and $Q_{\mathrm{gen},i}$ are the active and reactive power outputs of the generator at bus i, respectively; the superscripts min and max represent the lower and upper limits of the corresponding variables, respectively; κ_i^{P} and κ_i^{Q} are the active and reactive adjustment rates of bus i, respectively; P_{ij} and Q_{ij} are the active and reactive power flows of the line between buses i and j, respectively; G_{ij} and B_{ij} are the conductance and susceptance of the line between buses i and j, respectively; V_i and θ_i are the voltage amplitude and phase angle of bus i, respectively; and θ_{ij} is the difference of phase angle between buses i and j.

Constraints (26)-(28) mean that the active/reactive power input should be equal to the active/reactive power output at bus i. Constraints (29) and (30) mean that the up-regulation active/reactive power of generators is limited by the active/reactive adjustment rate and the maximum active/reactive power output of the generator at bus i. Constraints (31) and (32) mean that the down-regulation active/reactive power of generators is limited by the active/reactive adjustment rate and the minimum active/reactive power output of the generator at bus i. Constraints (33) and (34) denote the active/reactive power balance in power systems. Constraint (35) is the definition of the difference of phase angle between buses i and j.

Due to the thermal stability, voltage stability, and economic concerns, the power flow in transmission lines, bus voltage, and switch number of transmission lines are limited. Therefore, these physical limit constraints can be represented as:

$$0 \le P_{\mathrm{gen},i}^2 + Q_{\mathrm{gen},i}^2 \le (S_{\mathrm{gen},i}^{\max})^2 \quad (36)$$

$$I_{ij}^2 = (P_{ij}^2 + Q_{ij}^2)/V_i^2 \le y_{ij}(I_{ij}^{\max})^2 \quad (37)$$

$$V_i^{\min} \le V_i \le V_i^{\max} \quad (38)$$

$$N_{\mathrm{line}} - N_{\mathrm{cut}}^{\max} \le \sum_{i=1}^{N_{\mathrm{bus}}}\sum_{j=1}^{N_{\mathrm{bus}}} y_{ij}/2 \quad (39)$$

where $S_{\mathrm{gen},i}^{\max}$ and $I_{ij}^{\max}$ are the upper limits of apparent power of the generator at bus i and line current of the line between buses i and j, respectively; N_{line} and $N_{\mathrm{cut}}^{\max}$ are the number of lines on the normal operation (i.e., before controlled islanding) and the maximum number of lines that can be cut, respectively.

Constraint (36) denotes the safe operation limit of generators. Constraint (37) means that the current in the line between buses i and j cannot exceed its thermal limit. Constraint (38) means that the voltage at bus i should keep in its normal range. Constraint (39) means that breakers should not be triggered too frequently so as to reduce unnecessary economic losses.

F. Model Reformulation by SOC Relaxation

It can be seen that constraints (33), (34), and (37) are nonlinear and non-convex, so they cannot be efficiently solved by existing commercial solvers, and the optimality of the results cannot be guaranteed either. To deal with this issue, SOC relaxation, which is widely applied in the field of convex optimization and can determine the infimum of the original programming problem, is involved in this part to convert constraints (33), (34), and (37) into second-order form. The auxiliary variables α_{ij}, β_{ij}, $\hat{\gamma}_i$, $\hat{\gamma}_j$, γ_i, and γ_j are involved as:

$$\alpha_{ij} = y_{ij}V_iV_j\sin\theta_{ij} \approx y_{ij}\theta_{ij} \quad (40)$$

$$\beta_{ij} = y_{ij}V_iV_j\cos\theta_{ij} \quad (41)$$

$$\begin{cases} \hat{\gamma}_i = V_i^2 \\ \hat{\gamma}_j = V_j^2 \end{cases} \quad (42)$$

$$\begin{cases} \gamma_i = y_{ij}\hat{\gamma}_i \\ \gamma_j = y_{ij}\hat{\gamma}_j \end{cases} \quad (43)$$

It is noted that θ_{ij} would not be too large (≈ 0) in power systems, so $\sin\theta_{ij} \approx \theta_{ij}$ in constraint (40). Substitute constraints (40)-(43) to constraints (33), (34), (37), and (38), and we can obtain:

$$P_{ij} = \gamma_i G_{ij} - \beta_{ij}G_{ij} - \alpha_{ij}G_{ij} \quad (44)$$

$$Q_{ij} = \alpha_{ij}G_{ij} - \beta_{ij}B_{ij} - \gamma_i G_{ij} \quad (45)$$

$$(V_i^{\min})^2 \le \hat{\gamma}_i \le (V_i^{\max})^2 \quad (46)$$

$$(G_{ij}^2 + B_{ij}^2)(\gamma_i + \gamma_j - \beta_{ij}) \le y_{ij}(I_{ij}^{\max})^2 \quad (47)$$

It is noted that V_i, V_j and $\cos\theta_{ij}$ are included in constraint (41), thus they can be and should be replaced as:

$$\alpha_{ij}^2 + \beta_{ij}^2 = \gamma_i\gamma_j \quad (48)$$

However, constraint (48) is still non-convex. Therefore, the SOC relaxation is used to convert it into constraint (49), which would be further rearranged into the form of constraint (50).

$$\alpha_{ij}^2 + \beta_{ij}^2 \le \gamma_i\gamma_j \quad (49)$$

$$(2\alpha_{ij})^2 + (2\beta_{ij})^2 + (\gamma_i - \gamma_j)^2 \le (\gamma_i + \gamma_j)^2 \quad (50)$$

There is no doubt that relaxing the equality constraint into the inequality constraint would cause some errors, but the errors are demonstrated acceptable in [31]. So far, the variables V_i, V_j, $\sin\theta_{ij}$, and $\cos\theta_{ij}$ are eliminated and replaced by new auxiliary variables α_{ij}, β_{ij}, $\hat{\gamma}_i$, $\hat{\gamma}_j$, γ_i, and γ_j. Besides, all constraints except for (43) are in linear or SOC form. Thus, the "big-M" method [29], [30] is utilized again to linearize constraint (43) as:

$$-M(1-y_{ij}) \le \gamma_i - \hat{\gamma}_i \le M(1-y_{ij}) \quad (51)$$

$$-M(1-y_{ij}) \le \gamma_j - \hat{\gamma}_j \le M(1-y_{ij}) \quad (52)$$

G. Controlled Islanding Model Based on MISOCCP After Model Reformulation

After model reformulation, all chance constraints and nonlinear constraints are converted into linear or SOC form, and the controlled islanding model based on MISOCP and CCP models can be represented as the deterministic optimization programming. Thus, the final controlled islanding model based on MISOCCP can be represented as:

$$\begin{cases} \min \dfrac{1}{N_{\text{samp}}} \displaystyle\sum_{\lambda=1}^{N_{\text{samp}}} \sum_{i=1}^{N_{\text{bus}}} P_{\text{UB},i,\lambda} = \sum_{\lambda=1}^{N_{\text{samp}}} \sum_{i=1}^{N_{\text{bus}}} (P^{\text{up}}_{\text{gen},i,\lambda} + \tilde{P}_{\text{w},i,\lambda} + \tilde{P}_{\text{s},i,\lambda} - \tilde{P}_{\text{L},i,\lambda}) \\ \text{s.t. (6)-(10), (12), (13), (15)-(32), (35), (36), (38), (39), (44), (47), (50)-(52)} \end{cases} \quad (53)$$

III. Case Studies

A. Case Studies in Revised IEEE 39-bus Power System

The revised IEEE 39-bus power system is a simplification of the New England power system, and its single-line diagram is shown in Fig. 1.

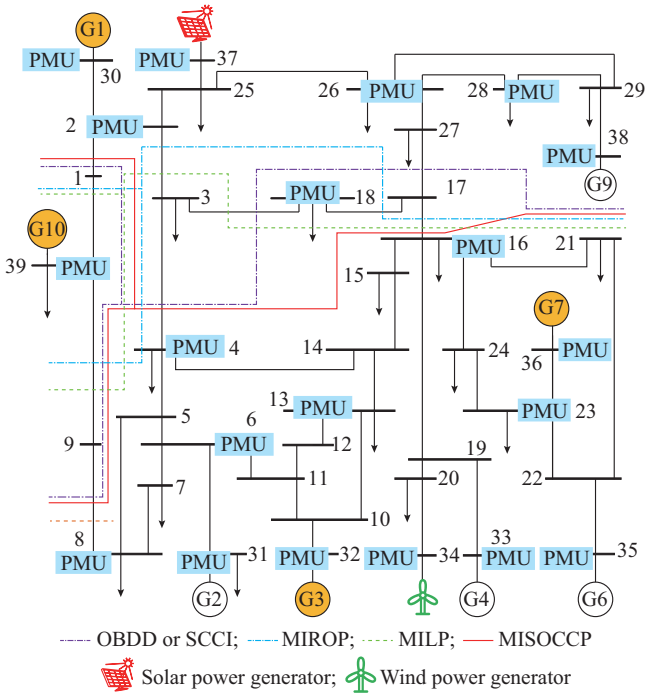

Fig. 1. Single-line diagram of revised IEEE 39-bus power system and islanding boundaries determined by different controlled islanding models.

To employ the proposed model, several assumptions are set in Table I, and it should be noted that the coherent generators assumed in this study are determined by the slow coherency method [6], the optimal PMU locations to maintain the observability of the power system are determined according to [32], and the minimum number of buses in each black-start zone $N_{\text{BS}}^{\min}$ is set as 3. In Fig. 1, the locations of black-start generators are labeled with orange. Once the islanding is required for the power system, the proposed model would be utilized and the results are shown in Table II, Fig. 1, and Fig. 2, where SCCI stands for spectral clustering controlled islanding. It can be observed that the power system is divided into three islands, and there would be 403.4 MW unbalanced power.

TABLE I
Initial Assumptions of Revised IEEE 39-bus Power System

Assumption	Bus No.
Location of black-start generators	30, 32, 36, 39
Location of wind power generators	37
Location of solar power generators	34
Transformer branch	6-31, 10-32, 19-33, 19-20, 2-30, 22-35, 25-37, 29-38, 20-34, 12-11, 12-13, 23-36
Coherent generator group [14]	{30, 37, 38}, {31, 32, 33, 34, 35, 36}, {39}
Optimal PMU location [32]	2, 4, 6, 8, 13, 16, 18, 23, 26, 28, 30, 31, 32, 33, 34, 35, 36, 37, 38, 39

TABLE II
Comparisons of Different Controlled Islanding Models for Revised IEEE 39-bus Power System Without Considering Uncertainty of RESs

Model	Islanding boundary	Island	Average unbalanced power (MW)	Unobserved bus
OBDD or SCCI	8-9, 3-4, 3-18, 17-27, 1-2	{4, 5, 6, 7, 8, 10, 11, 12, 13, 14, 15, 16, 17, 18, 19, 20, 21, 22, 23, 24, 31, 32, 33, 34, 35, 36}, {2, 3, 25, 26, 27, 28, 29, 30, 37, 38}, {1, 9, 39}	477.54	Null
MILP	9-39, 2-3, 3-18, 16-17, 1-39	{3, 4, 5, 6, 7, 8, 9, 10, 11, 12, 13, 14, 15, 16, 19, 20, 21, 22, 23, 24, 31, 32, 33, 34, 35, 36}, {2, 17, 18, 25, 26, 27, 28, 29, 30, 37, 38}, {1, 39}	653.85	Null
Proposed	1-2, 3-4, 8-9, 16-17	{6, 7, 8, 10, 11, 12, 13, 14, 15, 16, 19, 20, 21, 22, 23, 24, 31, 32, 33, 34, 35, 36}, {2, 3, 17, 18, 25, 26, 27, 28, 29, 30, 37, 38}, {1, 9, 39}	402.40	Null

To compare the effectiveness of the proposed model with other models, the results obtained by other models are also given in Table II, Table III, Fig. 1, and Fig. 2.

In Table II, the comparisons are associated with the optimization models that cannot deal with uncertain variables to show the importance of considering the uncertainty of RESs; while in Table III the comparisons are associated with the optimization models that consider the uncertainty of RESs, which is fairer for showing the effectiveness of the proposed model. In Table III, MIROP stands for mixed-integer robust

optimization programming. It is noted that different scenarios of fluctuations of RESs and loads would result in different unbalanced power, which is shown in Fig. 2. Additionally, the average unbalanced power of 1000 scenarios is shown in Table II and Table III. It can be observed that there is the same island for the OBDD, SCCI, and proposed models, i.e., {1, 9, 39}, while the other two islands are different. For the MILP and MIROP [19] models, all the three islands obtained are different from the ones obtained by the proposed model. Normally, a larger island is better for operation, since the possibility of maintaining the power balance will be greater [6]. For the MILP and MIROP models, the island {1, 39} is divided and there are only one generator bus and one load bus on this island, so there would be more unbalanced power with RESs considered in the majority of scenarios. Furthermore, it can be observed that there are the most and the second most unbalanced power in the MIROP and MILP models among the five models. For the OBDD [33] and SCCI [14] models, they are built for the power systems with traditional generations and do not consider the fluctuations of RESs and loads. Therefore, the results are also inferior to the results obtained by the proposed model.

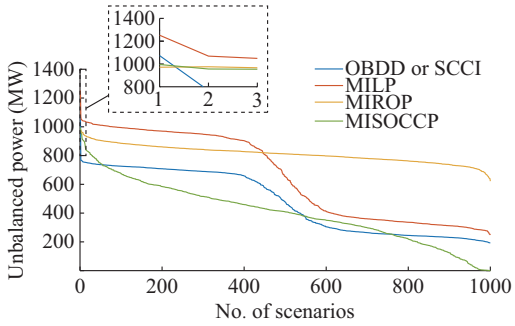

Fig. 2. Unbalanced power after islanding in revised IEEE 39-bus power system.

TABLE III
COMPARISONS OF DIFFERENT CONTROLLED ISLANDING MODELS FOR REVISED IEEE 39-BUS POWER SYSTEM CONSIDERING UNCERTAINTY OF RESS

Model	Islanding boundary	Island	Average unbalanced power (MW)	Unobserved bus
MIROP	9-39, 2-3, 17-18, 16-17, 1-39	{3, 4, 5, 6, 7, 8, 9, 10, 11, 12, 13, 14, 15, 16, 18, 19, 20, 21, 22, 23, 24, 31, 32, 33, 34, 35, 36}, {2, 17, 25, 26, 27, 28, 29, 30, 37, 38}, {1, 39}	811.34	17
Proposed	1-2, 3-4, 8-9, 16-17	{6, 7, 8, 10, 11, 12, 13, 14, 15, 16, 19, 20, 21, 22, 23, 24, 31, 32, 33, 34, 35, 36}, {2, 3, 17, 18, 25, 26, 27, 28, 29, 30, 37, 38}, {1, 9, 39}	402.40	Null

It is noted that although OBDD and SCCI models can obtain the same results for controlled islanding, they are two different models for controlled islanding. For the OBDD model, there are mainly three steps [9], [33]: ① reduce the search space by reducing nodes and branches of power systems; ② perform OBDD, which can quickly search for the feasible section; ③ verify the thermal and steady-state stability limit to obtain a smaller solution space. For the SCCI model, there are mainly two steps: ① use the normalized spectral clustering method to determine the coherent generators; ② divide all buses with the objective function of the minimum power flow disruption using constrained spectral clustering with the coherency and several general constraints. Another difference between the two models is that several solutions can be obtained by the OBDD model while only one solution can be obtained by the SCCI model, although the best solutions obtained by the OBDD model are the same as the one obtained by the SCCI model.

It can be observed from Fig. 2 that the curve shapes of OBDD, SCCI, and MILP models are different from the ones of MIROP and proposed models, i.e., they maintain relatively large values until around the 400th scenario. The reason is that the OBDD, SCCI, and MILP models do not consider the fluctuation of RESs and loads, which means they are the deterministic models, so large unbalanced power would be caused in numerous scenarios that have large fluctuations of RESs and loads. However, from another perspective, numerous scenarios have small fluctuations, so relatively small unbalanced power is caused in the other 600 scenarios. Since the power systems have certain power regulation abilities in general, relatively more scenarios belong to the latter one. Therefore, the unbalanced power caused by fluctuations of RESs and loads drops from around the 400th scenario.

It can also be observed that the MIROP and the proposed models obtain the least and the second least values regarding the maximum unbalanced power in 1000 scenarios, i.e., the values in the 1st scenario, when compared with other models. The reasons could be both the MIROP and proposed models can consider extreme situations of fluctuations of RESs and loads, and the MIROP model is the most robust one, which is able to handle the worst of the scenarios. In other words, the other models fail to consider the fluctuations of RESs and loads. Therefore, quite a large amount of unbalanced power would be caused under situations where RESs and loads fluctuate severely. Furthermore, because of the inherent robustness of the MIROP model [19], it can achieve less balanced power than that obtained by the proposed model for the most extreme situation.

However, the robustness, i.e., conservativeness, is also a drawback of the MIROP model from another point of view [20]. It is too conservative, which causes that the results obtained in the rest of most scenarios are not so good as those obtained by other models. For the MIROP model [19], the fluctuations, i.e., uncertainties, of RESs and loads are described by using the box uncertainty set, and it makes sure that the constraints would not be satisfied at a 100% confidence level. Obviously, the MIROP model is very robust but also extremely conservative. Therefore, its average unbalanced power is larger than that of the other four models, since it should guarantee that every constraint is satisfied in any scenario with any possible output of RESs. For the proposed model, the probabilities of different scenarios, i.e., different outputs of RESs, are described by the probability dis-

tribution, and the constraints are not needed to be satisfied strictly but at a certain confidence level. For example, the confidence level in this study is set to be 99%, which means that each constraint associated with RESs is needed to be satisfied at a 99% confidence level. The rationalities of this adjustment are: ① a small number of unsatisfied constraints, e.g., thermal limit, would not cause serious problems in power systems since there is a tolerance for the operation of power systems; ② the probability of the situations that make the constraints unsatisfied is quite small, and this trade-off for economic efficiency is worthwhile. Hence, the proposed model considers the uncertainties of RESs and loads comprehensively and outperforms the other four models in the revised IEEE 39-bus power system, which demonstrates its effectiveness.

B. Case Studies in Revised IEEE 118-bus Power System

The revised IEEE 118-bus power system is a simplified power system for the American electric power system in 1962. In this power system, there are 54 generators (35 of them are synchronous condensers), 186 line branches (7 of them are double circuit lines), 11 transformer branches, and 91 loads. To utilize this power system for demonstrating the proposed model, several assumptions are set in Table IV with $N_{\mathrm{BS}}^{\min}=20$, and some revisions are employed, i.e., generators at buses 12, 65, and 81 are revised as wind power generators and generators at buses 24 and 111 are revised as solar power generators, which are shown in Fig. 3. Besides, the coherent generator groups and PMU locations are determined according to [14] and [32], respectively.

By employing the proposed model, the islanding boundary and unbalanced power are determined and shown in Table V, Table VI, Fig. 3, and Fig. 4. The power system is divided into three parts, and the average unbalance power is 319.3 MW in 1000 scenarios when considering the fluctuations of RESs and loads. It can also be observed that there are more than 20 buses on each island and all the buses on each island are observable, which would benefit the back-up restoration measures.

TABLE IV
INITIAL ASSUMPTIONS OF REVISED IEEE 118-BUS POWER SYSTEM

Assumption	Bus No.
Location of black-start generators	10, 59, 100
Location of wind power generators	12, 65, 81
Location of solar power generators	24, 111
Transformer branch	86-87, 68-116, 8-5, 26-25, 30-17, 38-37, 63-59, 64-61, 65-66, 68-69, 81-80
Coherent generator group	{10, 12, 25, 26, 31}, {46, 49, 54, 59, 61, 65, 66, 69, 80}, {87, 89, 100, 103, 111}
PMU location	1, 5, 12, 13,17, 21, 23, 26, 28, 34, 37, 41, 45, 49, 53, 56, 62, 63, 68, 71, 75, 77, 80, 85, 86, 90, 94, 101, 105, 110, 114

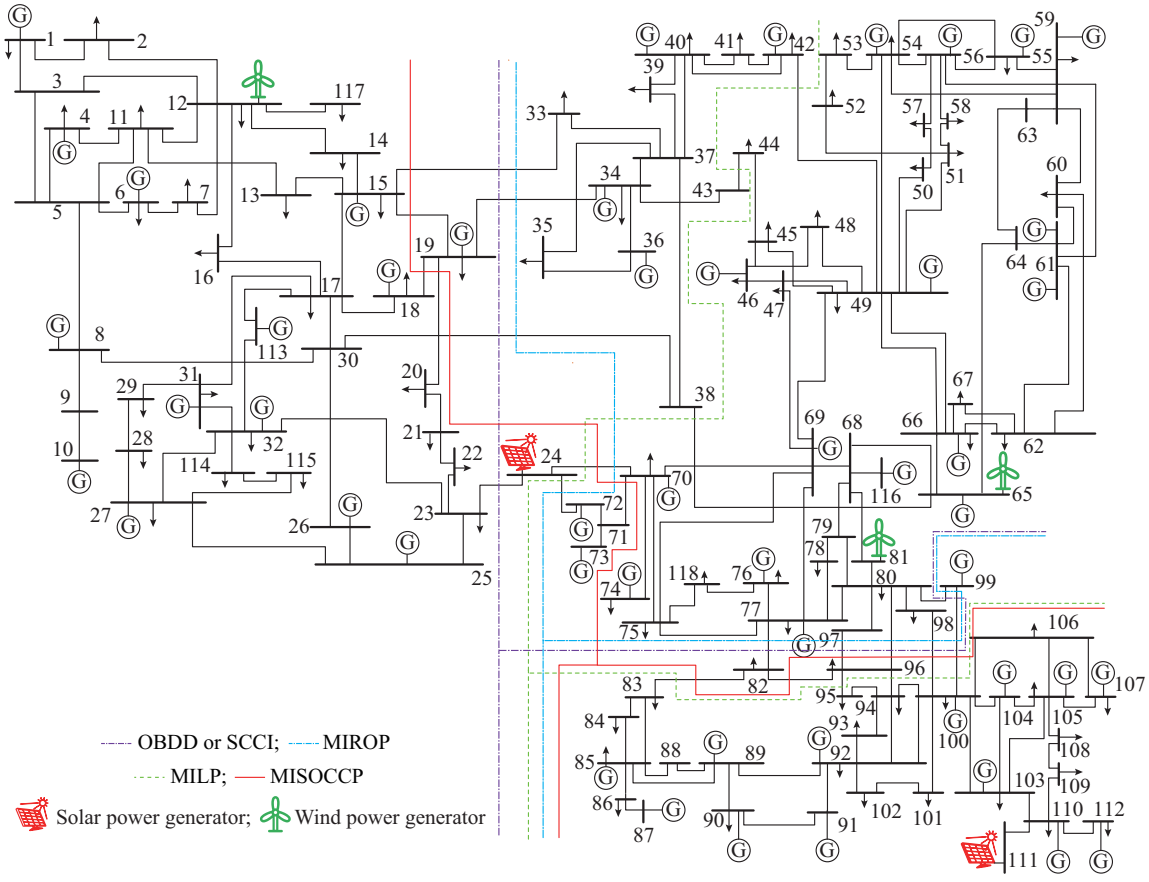

Fig. 3. Single-line diagram of revised IEEE 118-bus power system and islanding boundaries determined by different controlled islanding models.

Similarly, more comparisons are given in Table V and Table VI to demonstrate the importance of considering the uncertainty of RESs and the effectiveness of the proposed model.

TABLE V
COMPARISONS OF DIFFERENT CONTROLLED ISLANDING MODELS FOR REVISED IEEE 118-BUS POWER SYSTEM WITHOUT CONSIDERING UNCERTAINTY OF RESS AND LOADS

Model	Islanding boundary	Average unbalanced power (MW)	Unobserved bus
OBDD or SCCI	15-33, 19-34, 30-38, 23-24, 77-82, 96-97, 80-96, 98-100, 80-99	363.8	19, 24, 82
MILP	43-44, 42-49, 38-65, 24-70, 24-72, 82-83, 94-96, 95-96, 98-100, 99-100	538.7	42
Proposed	18-19, 19-20, 15-19, 15-33, 30-38, 24-70, 70-71, 82-83, 80-96, 82-96, 96-97, 98-100, 99-100	319.3	Null

TABLE VI
COMPARISONS OF DIFFERENT CONTROLLED ISLANDING MODELS FOR REVISED IEEE 118-BUS POWER SYSTEM CONSIDERING UNCERTAINTY OF RESS AND LOADS

Model	Islanding boundary	Average unbalanced power (MW)	Unobserved bus
MIROP	15-33, 19-34, 30-38, 24-70, 24-72, 77-82, 96-97, 80-96, 98-100, 80-99	573.1	19, 82
Proposed	18-19, 19-20, 15-19, 15-33, 30-38, 24-70, 70-71, 82-83, 80-96, 82-96, 96-97, 98-100, 99-100	319.3	Null

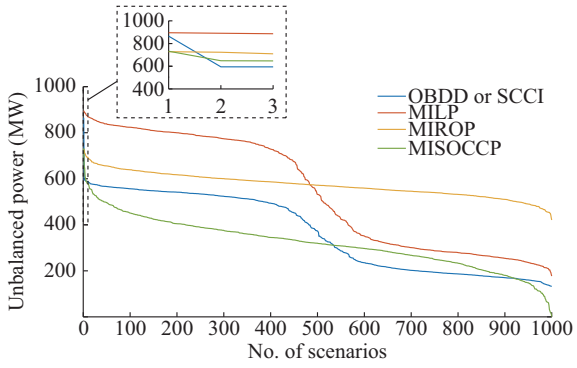

Fig. 4. Unbalanced power after islanding in revised IEEE 118-bus system.

For the OBBB and SCCI models, the unbalanced power is 363.8 MW and three buses, i.e., buses 19, 24, and 82, are unobservable. The reason for this is that the lines 19-34, 23-24, and 77-82 are disconnected by these islanding models, and buses 19, 24, and 82 cannot be observed since the nearest PMUs to them are exactly installed at buses 34, 23, and 77. For the MILP model, the unbalanced power is 538.7 MW, and bus 42 is unobservable after islanding since the line 42-49 is disconnected, and the nearest PMU to it is exactly installed at bus 49. For the MIROP model, the unbalanced power is the largest compared with the other models after islanding. In addition, buses 19 and 82 are unobservable. The reason is similar to the ones of OBDD, SCCI, and MILP models. It can also be observed from Fig. 4 that the curve shapes have similar features with regard to the ones of revised IEEE 39-bus system, which illustrates that the MIROP and proposed models can consider the influence of RESs, and the proposed model is less conservative once again.

It can be observed from Fig. 3 that the solar power generator at bus 24 and the wind power generator at bus 81 are near the islanding boundaries determined by the five models. It should be noted that RES would involve the fluctuations in power systems, and traditional generators and synchronous condensers would be helpful to mitigate the fluctuations. For the solar power generator at bus 24, synchronous condensers at buses 72 and 73 are the nearest ones. The islanding boundaries determined by the OBDD, SCCI, and proposed models cluster buses 24, 72, and 73 into the same island, which means the fluctuations of the solar power generator could be mitigated by the synchronous condensers at buses 72 and 73. Hence, the OBDD, SCCI, and the proposed models result in less unbalanced power than the MIROP model in this case. Similarly, the nearest synchronous condenser, i.e., synchronous condenser at bus 99, is assigned to the same island by the MIROP and proposed models, and the wind power generator is connected at bus 81. Therefore, the proposed model results in less unbalanced power than the OBDD and SCCI models in this case.

IV. CONCLUSION

In this study, a controlled islanding model based on MISOCCP is proposed considering the uncertainty of RESs and loads. The uncertainties of RESs and loads are characterized by the possibility distribution models, i.e., Weibull, Beta, and Gaussian distribution models, with chance constraints, which are handled by the deterministic conversion method based on LLN to convert them into deterministic constraints. The non-convex islanding model is then converted into a convex optimization by SOC relaxation, which can be solved efficiently by commercial solvers. Case studies on two IEEE power systems show that the proposed model can divide the power system into several islands with the minimum unbalanced power and all buses observed, which is more meaningful and better than other controlled islanding models.

In summary, it can be concluded that: ① less unbalanced power would be caused by the proposed model compared with other models, since the MIROP model considers the uncertainty of RESs too conservatively, and the other three models are unable to consider the uncertainty of RESs; ② the islanding boundary and corresponding islands determined by the proposed model are more suitable than the ones determined by other models, since the observability of each bus on the island can be guaranteed, which is beneficial for operators to perform back-up load restoration; ③ the unbalanced power after islanding is strongly associated with the locations of RESs while assigning the nearest traditional generators or synchronous condensers into the same island would

mitigate the unbalanced power.

REFERENCES

[1] S. Liu, Y. Zhao, Z. Lin *et al*., "Data-driven event detection of power systems based on unequal-interval reduction of PMU data and local outlier factor," *IEEE Transactions on Smart Grid*, vol. 10, no. 11, pp. 1630-1643, Mar. 2020.

[2] K. Sun, K. Li, J. Pan *et al*., "An optimal combined operation scheme for pumped storage and hybrid wind-photovoltaic complementary power generation system," *Applied Energy*, vol. 242, pp. 1155-1163, May 2019.

[3] T. Zhang, S. Liu, W Qiu *et al*., "KPI-based real-time situational awareness for power systems with high proportion of renewable energy sources," *CSEE Journal of Power and Energy Systems*. doi: 10.17775/CSEEJPES.2020.01530

[4] H. You, V. Vittal, and X. Wang, "Slow coherency-based islanding," *IEEE Transactions on Power Systems*, vol. 19, no. 1, pp. 483-491, Feb. 2004.

[5] B. Yang, V. Vittal, and G. T. Heydt, "Slow-coherency-based controlled islanding – a demonstration of the approach on the August 14, 2003 blackout scenario," *IEEE Transactions on Power Systems*, vol. 21, no. 4, pp. 1840-1847, Nov. 2006.

[6] G. Xu and V. Vittal, "Slow coherency based cutset determination algorithm for large power systems," *IEEE Transactions on Power Systems*, vol. 25, no. 2, pp. 877-884, May 2010.

[7] F. Znidi, H. Davarikia, K. Iqbal *et al*., "Multi-layer spectral clustering approach to intentional islanding in bulk power systems," *Journal of Modern Power Systems and Clean Energy*, vol. 7, no. 5, pp. 1044-1055, Jul. 2019.

[8] M. R. Aghamohammadi and A. Shahmohammadi, "Intentional islanding using a new algorithm based on ant search mechanism," *International Journal of Electrical Power & Energy Systems*, vol. 35, no. 1, pp. 138-147, Feb. 2012.

[9] K. Sun, D. Zheng, and Q. Lu, "Splitting strategies for islanding operation of large-scale power systems using OBDD-based methods," *IEEE Transactions on Power Systems*, vol. 18, no. 2, pp. 912-923, May 2003.

[10] F. Teymouri, T. Amraee, H. Saberi *et al*., "Towards controlled islanding for enhancing power grid resilience considering frequency stability constraints," *IEEE Transactions on Smart Grid*, vol. 10, no. 2, pp. 1735-1746, Mar. 2019.

[11] A. Kyriacou, P. Demetriou, C. Panayiotou *et al*., "Controlled islanding solution for large-scale power systems," *IEEE Transactions on Power Systems*, vol. 33, no. 2, pp. 1591-1602, Mar. 2018.

[12] T. Ding, K. Sun, C. Huang *et al*., "Mixed-integer linear programming-based splitting strategies for power system islanding operation considering network connectivity," *IEEE Systems Journal*, vol. 12, no. 1, pp. 350-359, Mar. 2018.

[13] M. Padhee, P. K. Dash, K. R. Krishnanand *et al*., "A fast Gauss-Newton algorithm for islanding detection in distributed generation," *IEEE Transactions on Smart Grid*, vol. 3, no. 3, pp. 1181-1191, Sept. 2012.

[14] L. Ding, F. M. Gonzalez-Longatt, P. Wall *et al*., "Two-step spectral clustering controlled islanding algorithm," *IEEE Transactions on Power Systems*, vol. 28, no. 1, pp. 75-84, Feb. 2013.

[15] S. Admasie, S. B. A. Bukhari, T. Gush *et al*., "Intelligent islanding detection of multi-distributed generation using artificial neural network based on intrinsic mode function feature," *Journal of Modern Power Systems and Clean Energy*, vol. 8, no. 3, pp. 511-520, May 2020.

[16] Y. Park and J. Park, "Robust optimal scheduling with a grid-connected microgrid installed in a large-scale power consumer," *Journal of Electrical Engineering & Technology*, vol. 14, no. 5, pp. 1881-1892, Jul. 2019.

[17] Y. Xu, Q. Guo, H. Sun *et al*., "Distributed discrete robust secondary cooperative control for islanded microgrids," *IEEE Transactions on Smart Grid*, vol. 10, no. 4, pp. 3620-3629, Jul. 2019.

[18] G. Liu, M. Starke, B. Xiao *et al*., "Robust optimisation-based microgrid scheduling with islanding constraints," *IET Generation, Transmission & Distribution*, vol. 11, no. 7, pp. 1820-1828, May 2017.

[19] S. Liu, Z. Lin, Y. Zhao *et al*., "Robust system separation strategy considering online wide-area coherency identification and uncertainties of renewable energy sources," *IEEE Transactions on Power System*, vol. 35, no. 5, pp. 3574-3587, Sept. 2020.

[20] Y. Zhang, J. Wang, B. Zeng *et al*., "Chance-constrained two-stage unit commitment under uncertain load and wind power output using bilinear benders decomposition," *IEEE Transactions on Power Systems*, vol. 32, no. 5, pp. 3637-3647, Sept. 2017.

[21] J. K. Sengupta, "Stochastic linear programming with chance constraints," *International Economic Review*, vol. 11, no. 1, pp. 101-116, Feb. 1970.

[22] Y. Yuan, Z. Li, and B. Huang, "Robust optimization approximation for joint chance constrained optimization problem," *Journal of Global Optimization*, vol. 67, pp. 805-827, Apr. 2017.

[23] M. Ismail, A. E. Hefnawy, and A. E. Saad, "New deterministic solution to a chance constrained linear programming model with Weibull random coefficients," *Future Business Journal*, vol. 4, no. 1, pp. 109-120, Jun. 2018.

[24] D. Michel, *A Modern Introduction to Probability and Statistics*. New York: Springer, 2005.

[25] K. Yao and J. Gao, "Law of large numbers for uncertain random variables," *IEEE Transactions on Fuzzy Systems*, vol. 24, no. 3, pp. 615-621, Jun. 2016.

[26] B. Hu, Y. Li, H. Yang *et al*., "Wind speed model based on kernel density estimation and its application in reliability assessment of generating systems," *Journal of Modern Power Systems and Clean Energy*, vol. 5, no. 2, pp. 220-227, May 2017.

[27] J. Prada and J. R. Dorronsoro, "General noise support vector regression with non-constant uncertainty intervals for solar radiation prediction," *Journal of Modern Power Systems and Clean Energy*, vol. 6, no. 2, pp. 268-280, Mar. 2018.

[28] M. Nijhuis, M. Gibescu, and S. Cobben, "Gaussian mixture based probabilistic load flow for LV-network planning," *IEEE Transactions on Power Systems*, vol. 32, no. 4, pp. 2878-2886, Jul. 2017.

[29] W. L. Winston, *Operations Research: Applications and Algorithms*. 4th ed., Boston: Cengage Learning, 2003.

[30] J. Lofberg, "YALMIP: a toolbox for modeling and optimization in MATLAB," in *Proceedings of the IEEE International Symposium on Computer-Aided Control System Design*, Taipei, China, Sept. 2004, pp. 284-289.

[31] T. Ding, K. Sun, Q. Yang *et al*., "Mixed integer second order cone relaxation with dynamic simulation for proper power system islanding operations," *IEEE Journal on Emerging and Selected Topics in Circuits and Systems*, vol. 7, no. 2, pp. 295-306, Jun. 2017.

[32] P. Demetriou, M. Asprou, and E. Kyriakides, "A real-time controlled islanding and restoration scheme based on estimated states," *IEEE Transactions on Power Systems*, vol. 34, no. 1, pp. 606-615, Jan. 2019.

[33] K. Sun, K. Hur, and P. Zhang, "A new unified scheme for controlled power system separation using synchronized phasor measurements," *IEEE Transactions on Power Systems*, vol. 26, no. 3, pp. 1544-1554, Aug. 2011.

Shengyuan Liu received the B. E. degree in electrical engineering from Shandong University, Jinan, China, in 2017. He is currently pursuing the Ph. D. degree in the College of Electrical Engineering, Zhejiang University, Hangzhou, China. He is also a visiting Ph. D. student at The University of Tennessee, Knoxville, USA, from 2019 to 2020. His research interests include wide area monitoring and control of power systems, situation awareness of power systems, and data-driven approaches in power systems.

Tianhan Zhang received the B.E. degree in the College of Electrical Engineering, Zhejiang University, Hangzhou, China, in 2019. He is currently working toward the Ph. D. degree in the College of Electrical Engineering, Zhejiang University. His research interests include power system situation awareness and application of blockchain in power system.

Zhenzhi Lin received the Ph.D. degree in electrical engineering from South China University of Technology, Guangzhou, China, in 2008. He was a Research Assistant in the Department of Electrical Engineering at The Hong Kong Polytechnic University, Hong Kong, China, from 2007 to 2008, a Research Scholar in the Department of Electrical Engineering and Computer Science at the University of Tennessee, Knoxville, USA, from 2010 to 2011, and a Research Associate in College of Engineering and Computing Sciences at Durham University, Durham, UK, from 2013 to 2014. He is currently a Professor in the College of Electrical Engineering, Zhejiang University, Hangzhou, China. His research interests include power system wide-area monitoring and control, controlled islanding and power system restoration, and data mining in power systems.

Yilu Liu received the B. S. degree from Xi'an Jiaotong University, Xi'an, China, and the M.S. and Ph.D. degrees from the Ohio State University, Columbus, USA, in 1986 and 1989, respectively. She was currently the Gover-

nor's Chair with the University of Tennessee (UTK), Knoxville, USA, and Oak Ridge National Laboratory (ORNL), Oak Ridge, USA. She is elected as the Member of National Academy of Engineering in 2016. She is also the Deputy Director of the DOE/NSF Co-funded Engineering Research Center CURENT. Prior to joining UTK/ORNL, she was a Professor at Virginia Polytechnic Institute and State University, Blacksburg, USA. Her current research interests include power system wide-area monitoring and control, large interconnection-level dynamic simulations, electromagnetic transient analysis, and power transformer modeling and diagnosis.

Yi Ding received the B.Eng. degree from Shanghai Jiao Tong University, Shanghai, China, in 2000, and the Ph.D. degree from Nanyang Technological University (NTU), Singapore, in 2007, both in electrical engineering. He is a Professor in the College of Electrical Engineering, Zhejiang University (ZJU), Hangzhou, China. Before joining ZJU, he was an Associate Professor in the Department of Electrical Engineering, Technical University of Denmark (DTU), Copenhagen, Denmark. He also held research and teaching positions in University of Alberta, Edmonton, Canada and NTU. He was a Consultant as Energy Economist for Asian Development Bank in 2010. He is an Editorial Member of international journals of Electric Power Systems Research and Journal of Modern Power Systems and Clean Energy. He is also a Guest Editor for the special section of IEEE Transactions on Power Systems. He is a Member of IEC working groups for micro-grid standards. His research interests include power system planning and reliability evaluation, smart grid and complex system risk assessment.

Li Yang received the Ph.D. degree in electrical engineering from Zhejiang University, Hangzhou, China, in 2004. She was a Post Doctorate in the Department of Electrical Engineering at Turin Polytechnic University, Turin, Italy, from 2007 to 2008. She is currently an Associate Professor in the College of Electrical Engineering, Zhejiang University. Her research interests include power market, power system economics and distribution network planning.